
KEEC: KOOPMAN EMBED TO CONTROL ON AN EQUIVARIANT GEOMETRY

A PREPRINT

Xiaoyuan Cheng[†]

Department of Civil, Environmental
& Geomatic Engineering
University College London
London, WC1E 6BT, UK

Yiming Yang[†]

Department of Statistical Science
University College London
London WC1E 6BT, UK

Wei Jiang

Department of Electrical
Engineering & Automation
Aalto University
Espoo 02150, Finland

Yukun Hu^{*}

University College London
Department of Civil, Environmental
& Geomatic Engineering
University College London
London, WC1E 6BT, UK

December 12, 2023

ABSTRACT

This paper investigates how representation learning can enable optimal control in unknown and complex dynamics, such as chaotic and non-linear systems, without relying on prior domain knowledge of the dynamics. The core idea is to establish an equivariant geometry that is diffeomorphic to the manifold defined by a dynamical system and to perform optimal control within this corresponding geometry, which is a non-trivial task. To address this challenge, Koopman Embed to Equivariant Control (KEEC) is proposed for model learning and control. Inspired by Lie theory, KEEC begins by learning a non-linear dynamical system defined on a manifold and embedding trajectories into a Lie group. Subsequently, KEEC formulates an equivariant value function equation in reinforcement learning on the equivariant geometry, ensuring an invariant effect as the value function on the original manifold. By deriving analytical-form optimal actions on the equivariant value function, KEEC theoretically achieves quadratic convergence for the optimal equivariant value function by leveraging the differential information on the equivariant geometry. The effectiveness of KEEC is demonstrated in challenging dynamical systems, including chaotic ones like Lorenz-63. Notably, our results show that isometric functions, which maintain the compactness and completeness of geometry while preserving metric and differential information, consistently outperform loss functions lacking these characteristics.

Keywords Koopman operator · Embed to control · Equivariant geometry · Optimal control · Unstable steady state

1 Introduction

The success of the model-based control approaches highly relies on the accuracy of the learned environmental model [1, 2]. However, characterizing an unknown control system directly from raw data, which can be attributed to the nonlinear structure, is challenging. Even though a satisfied model could be obtained, the model is often highly nonlinear, where model-based optimal control can be both analytically and computationally intractable. Both problems could, in principle, be addressed by finding a proper representation of the underlying dynamical system, which means it is possible for the dynamical system to evolve a *locally linearly* on the manifold and then robustly and easily perform

[†]These authors contributed equally to this work.

^{*}Corresponding author: yukun.hu@ucl.ac.uk

optimal control under an appropriate representation. Generally, discovering and controlling such a manifold is a non-trivial task for representation and learning.

To address this challenge, the concept of *Embed to Control* (E2C) was initially introduced in [3] to tackle stochastic optimal control by revealing the latent dynamics from raw images. In E2C, a proper transformation of pixel data using variational auto-encoders (VAE) into a latent space is performed, enabling the construction of a probabilistic generative model for long-term planning in the latent space. Alternative methods have been proposed to solve the control problem with unknown dynamics, most of which fall into the E2C class. Some researchers control the unknown systems by learning differential equations as the governing dynamics. For example, [4] proposes an ordinary differential equation (ODE) to govern and control Hamiltonian dynamics, while [5] presents a way to learn the Neural-ODE by state observer data, which can be understood as latent space. Regardless of the transformation of trajectory data into latent space, the learned dynamics should remain consistent with the original ones. Other methods, such as [6, 7], learn latent dynamics from raw images, which can be naturally classified as E2C. The conditions for keeping the latent dynamics faithful to the original ones are not explicitly given in the previous methods. Nevertheless, it should ensure that the transformed latent space retains symmetry and equivariance with respect to the original space under a group action. Recent research has highlighted the significance of the symmetric and equivariant representation of dynamical systems [8, 9, 10], demonstrating their effectiveness and efficiency in various applications, e.g., vision-based tasks [11, 12] and Markov Decision Processes (MDP) [13, 14, 15]. These prior works primarily focused on control tasks characterized by clear symmetries, such as rotation invariance and translation invariance. For example, [12] showcases an example of invariant rotation group action on the special orthogonal group ($SO(2)$) in a robotics control task, while [15] exploits the symmetric relationship between the left and right half-planes to reduce the size of the action space. Those methods can be effective in some scenarios with obvious symmetries. However, the symmetric relationship behind some raw data is not obvious, and constructing an equivariant dynamical system becomes the foundation of success for E2C.

To address this further challenge, some researchers proposed symmetry learning from another perspective. [16, 17] offered a meta-sequential prediction with an implicit disentanglement framework. This method achieves disentanglement as a by-product of training a model that can predict the future linearly in the latent space. Similar to the core idea of [16, 17], we found that the latent symmetry has a natural connection with the Koopman operator. This research is centred on employing an equivariant dynamical system for achieving E2C. Drawing inspiration from the group representation theory, we propose a novel algorithm called Koopman Embed to Equivariant Control (KEEC) to enable optimal control through Koopman operator theory without prior knowledge of the underlying dynamical systems.

The Koopman operator theory, initially proposed in [18] and [19] for Hamiltonian dynamical systems, forms the foundation of our approach. The central concept of this operator is to map the state of a nonlinear dynamical system to an embedding space where linear propagation into the future is feasible. Notably, the dynamical system remains invariant between the embedding space and the original space under the group action. Over the past few decades, the applications of the Koopman operator have gained significant attention. It has been broadly applied for two primary purposes: model learning and control tasks. In the realm of system prediction, many algorithms fall within the category of Dynamic Mode Decomposition (DMD) to learn the Koopman spectra [20, 21, 22] for uncontrolled dynamical systems. Some recent works have extended this method to control real-world systems, including robotics [23, 24, 25], and simulated fluid systems [26], with remarkable precision. Koopman operator theory can also be involved in some control frameworks, such as data-driven model predictive control (MPC) and reinforcement learning (RL), to improve the model performance. For example, [27] proposed a modified version of the Koopman operator to compute an extended state space by lifting the original state space to the product state and action space. The modified Koopman predictors can be used to design MPC controllers for nonlinear dynamical systems, and the computational complexity of the framework can be comparable to the MPC for linear dynamical systems. Another intriguing work by [28] delves into the symmetric and equivariant properties of the Koopman operator within Lie theory, proposing the use of offline RL to learn the Koopman operator. This well-trained operator can be used for data augmentation and integrated with classical online RL algorithms. However, it's important to note that these works primarily leverage the transformation-invariant property of the Koopman operator to generate the subsequent state information in the latent space directly without considering the geometric structure of the induced space. To the best of the authors' knowledge, no research has delved into learning the Koopman operator's differential form to enhance the efficiency and effectiveness of E2C. This paper demonstrates KEEC on the Swing-up Pendulum and Lorenz-63 stabilization tasks, where exploring the optimal action is equivalent to searching the optimal path on the induced Koopman geometry. In this paper, the KEEC proposed is fundamentally different from previous work. Our contributions can be summarized as follows:

- The establishment of a Lie group induced by the Koopman operator that is diffeomorphic to the original manifold of the dynamical system is demonstrated. The differential form of the Lie group is learned based on the isometric and isomorphic properties, which keeps the invariant metric information on the Lie group, see Lemma 1 and Theorem 1.

- An equivariant value function defined on a Lie group (see Theorem 1) is proposed, which can achieve invariance effects with the original manifold.
- The analytical form of optimal actions on equivariant value functions is derived from the first-order differential information of Lie groups. Equivariant value functions exhibit quadratic convergence rates (see Theorem 2 and 3).
- Isometric and isomorphic loss functions were found to be superior to non-isometric loss functions, and ensuring isometric and isomorphic properties is critical to maintaining the invariance of the underlying geometry (see Figure 1).
- The experiments indicate that our methods can achieve a higher reward with low variance in nonlinear and chaotic dynamics such as the Swing-up Pendulum and Lorenz-63.

In summary, the structure of this paper can be outlined as follows. Section 2 begins with an introductory overview of the Koopman operator and the fundamental control framework, MPC-based RL. Then, the connection between Lie theory and the Koopman operator is underscored, and a geometric perspective is provided. This representation of the Koopman operator leads to the induction of an equivariant value function. Section 3 gives the learning framework of KEEC and lays a theoretical foundation to ensure convergence and optimality. Furthermore, the role of the proposed KEEC in stabilizing two challenging dynamical systems is evaluated and compared with three types of benchmark control algorithms. Section 4 gives specific evaluation results and experiment details. Finally, Section 5 consists of a concluding discussion and future directions.

2 Preliminaries and Background

This section outlines the control objectives and theoretical foundation in our proposed learning framework, including an introduction to the MPC-based RL framework and concepts related to equivalence and symmetry.

2.1 Notions

\mathcal{H} denotes the Hilbert space, and $\mathcal{X} \mapsto \mathcal{H}(\mathcal{X})$ denotes that mapping from \mathcal{X} to the corresponding Hilbert space. G denotes a group, and GL is the generalized linear group. The symbols \mathfrak{g} and \mathcal{L} denote the Lie algebra and Lie derivative, respectively. And subscript \square_* and superscript \square^* are pushforward and pullback symbols, respectively. $Hom(\cdot, \cdot)$ is defined as the homomorphic category.

2.2 Main Assumptions

- The continuity and regularity of the dynamical system.** Assuming the differentiability of the dynamical system lies in C^1 , an equivariant geometry can be established that is diffeomorphic to the original manifold defined on the original dynamical system.
- The ergodicity of the dynamical system.** Assuming ergodicity, where the dynamical system is measure-preserving, enables the learning of dynamics using an invariant operator.
- The Koopman operator is block-wise reducible.** It is essential to assume that the Koopman operator is block-wise reducible, as equivariant functions are transferred under an adjoint map $Ad_g(h) = ghg^{-1}$.

2.3 Control Framework

Unknown dynamical system. This research aims to solve optimal control problems by performing on an equivariant geometry. Consider any unknown controlled dynamical system as

$$\dot{s} = f(s, a), \quad (1)$$

where $s \in \mathcal{S} \subset \mathbb{R}^n$ and $a \in \mathcal{A} \subset \mathbb{R}^m$ are the state and action, respectively. The dot stands for derivative with respect to (w.r.t.) t . Assuming that $f \in C^1((\mathbb{R}^n, \mathbb{R}^m), \mathbb{R}^n)$ is the 1-order differentiable (see Assumption (a)), the path integral of Equation (1) can be written as:

$$s_{T+\Delta t} = F(s_T, a_T) = \underbrace{s_T + f(s_T, a_T)\Delta t + \mathcal{O}(\Delta t^2)}_{\text{Taylor expansion of dynamical system}}, \quad (2)$$

where $s_{T+\Delta t}$ can be calculated by the function F , typically $s_{T+\Delta t}$ is determined by the current state s_T and action a_T .

MPC-based RL. Based on the definition of a dynamical system in Equations (1) and (2), this work considers a finite horizon model-based RL decision-making problem in an unknown dynamical system environment. The sequential

action $\{a_\tau\}$ is determined by a policy $\pi(\cdot | s_\tau)$, the target is to maximize the expected accumulated reward $r : \mathcal{S} \rightarrow \mathbb{R}$ in the future, such that

$$V^\pi(s_T) = \mathbb{E}[\sum_{\tau} \gamma^i r(s_\tau, a_\tau) | s_T, a_\tau \sim \pi], \quad \forall s_T \in \mathcal{S}, \quad (3)$$

where $V^\pi : \mathcal{S} \rightarrow \mathbb{R}$ is the value function to measure the future expected accumulated reward for the arbitrary state, $\gamma \in (0, 1)$ is the discounted factor, and $\forall s_0 \in \mathcal{S}$ is the initial state. In this paper, MPC is introduced as the basic control framework of RL [29, 30]. The target of MPC-based RL is to search an action sequence as a control policy over a finite horizon, which is denoted as $a_{T:T+(N-1)\Delta t} = (a_T, a_{T+\Delta t}, \dots, a_{T+(N-1)\Delta t})$. The corresponding value function under the MPC background can be defined as:

$$\underbrace{a_{T:T+(N-1)\Delta t}^*}_{\text{search optimal policy for } N\text{-step rollout}} \in \arg \max E[\underbrace{\sum_{\tau=T}^{T+(N-1)\Delta t} \gamma^i r(s_\tau, a_\tau)}_{N\text{-step rollout}} + \gamma^N V(s_{T+N\Delta t})], \quad (4)$$

$$\text{s.t. } s_{\tau+\Delta t} = F(s_\tau, a_\tau) \quad \forall \tau \in \{T, T + \Delta t, \dots, T + (N - 1)\Delta t\},$$

$$\forall a_\tau \in \mathcal{A}.$$

Computing the traditional MPC is complex when the model is unknown. Instead of the traditional dynamic programming method, we propose an equivariant value function which is equivalent to the original value function, in which an analytical solution for the optimal sequential action $a_{T:T+(N-1)\Delta t}^*$ can be derived. Before that, concepts related to equivariant representation need to be introduced, let's start from the basics of group representations.

2.4 Group Representation and Equivariant Function

The definitions of a group and other related concepts are given in Appendix A.

Definition 1. (Group representation) [31] A representation of a Lie group G is a vector space V together with a morphism $\rho : G \rightarrow GL(V)$. A representation of a Lie algebra \mathfrak{g} is a vector space V together with a morphism $\rho_* : \mathfrak{g} \rightarrow \mathfrak{gl}(V)$.

A morphism between two representations V, W of the group G is a linear map $f : V \rightarrow W$ with commutes with the action of $G : f\rho(g) = \rho(g)f$. The space of all G -morphisms between V and W will be denoted by $Hom_G(V, W)$. Similarly, one defines a morphism of representations of Lie algebra, with the symbol as $Hom_{\mathfrak{g}}(V, W)$. In the simply-connected manifold, the relationship holds such that $Hom_G(V, W) = Hom_{\mathfrak{g}}(V, W)$. The representation theory provides a symmetric way to represent the function $f = \rho(g)^{-1}f\rho(g)$. By introducing the lifted Lie algebra, the differential form of a dynamical system can be expressed in a diffeomorphism manner.

Definition 2. (Equivariant function) A function $f : V \rightarrow W$ is equivariant w.r.t. a representation of G if it commutes with the group transformation $g \in G$ such that

$$f(\rho(g)v) = \rho(g)f(v), \forall v \in V. \quad (5)$$

Obviously, the definition of equivariant function is directly developed from the group representation. The two definitions will be essential to representing a dynamical system in different spaces. Sometimes, the original space is difficult to tackle due to the nonlinearity. The equivariant representation provides an isomorphic way to transfer the original manifold to another space so that the dynamical system in the other space can be controlled, but the invariant value is preserved. The next section will connect the Koopman operator with the representation theory to give an equivariant representation of the dynamical system.

3 Learning Framework of KEEC

This section emphasizes presenting the fundamental algorithm structure of KEEC and the associated theorems. The outline of this section is:

- Commencing from framing the controlled dynamics within the Koopman operator representation in Subsection 3.1 and Appendix B, the discussion progresses to the acquisition of the equivariant geometry induced by transitive group action.
- The dynamics of the equivariant geometry are presented in Subsection 3.2, illustrating the construction of an equivariant value function that mirrors the invariance properties of the original value function. The corresponding loss functions established on the isometric and isomorphic properties are also given.
- An analytical-from optimal policy is derived on the equivariant geometry, which guarantees a quadratic convergence of the equivariant value function.
- Subsection 3.4 concludes by detailing the implementation of KEEC.

3.1 Controlled Dynamics and Koopman Operator

The original Koopman operator can be traced back to the pioneering work in [18]. It provides a lens through which to transform a Hamiltonian dynamical system into an embedded form within a Hilbert space via a linear transformation. The original system in [18] is an uncontrolled dynamical system. Following the canonical definition, the Koopman operator is extended to controlled dynamical systems.

Definition 3. (Koopman Operator) [32]. Let $(s, a) \mapsto g(s, a) \in \mathcal{H}(\mathcal{S}, \mathcal{A}), \forall s \in \mathcal{S}, a \in \mathcal{A}$ be a generalized infinite-dimensional Hilbert space. There exists a Koopman operator $\mathcal{K}_{\Delta t} : \mathcal{H}(\mathcal{S}, \mathcal{A}) \rightarrow \mathcal{H}(\mathcal{S}, \mathcal{A})$ that can be represented as:

$$\mathcal{K}_{\Delta t}g = g \circ F_{\Delta t}, \quad (6)$$

where \circ is the composition symbol, $F(\cdot, \cdot)$ is denoted as $F_{\Delta t}$. The Koopman operator is defined on a continuum, which is discretization-invariance [33]. For the arbitrarily small time interval Δt , it can derive the following property as

$$\mathcal{K}_{\Delta t}g(s_T, a_T) = g(F_{\Delta t}(s_T, a_T)) = g(F_{\Delta t}(s_T, a_T), a_{T+\Delta t}) = g(s_{T+\Delta t}, a_{T+\Delta t}). \quad (7)$$

More specifically, the $g(s_T, a_T)$ is called the “observables” and the Koopman operator $\mathcal{K}_{\Delta t}$ is an infinite dimensional operator which pushes the current observables $g(s_T, a_T)$ forward to $g(s_{T+\Delta t}, a_{T+\Delta t})$.

Remark 1. The Koopman operator inherits several advantageous properties from Hilbert space. As a result, it is essential to identify and elucidate these properties.

- (The homogeneity of Koopman [18]) The Koopman operator is linear from a spectral perspective; then naturally inherited the homogeneity in functional space:

$$\mathcal{K}_{\Delta t}(\alpha g_1 + \beta g_2) = \alpha g_1 \circ F_{\Delta t} + \beta g_2 \circ F_{\Delta t}. \quad (8)$$

- (Semi-group property ¹) The forward dynamics under the Koopman can be represented as a semi-group such that

$$\begin{aligned} & \mathcal{K}_{\Delta t_1 + \Delta t_2}g \\ &= \mathcal{K}_{\Delta t_1}\mathcal{K}_{\Delta t_2}g \\ &= \mathcal{K}_{\Delta t_1}g \circ F_{\Delta t_2} \\ &= g \circ F_{\Delta t_1} \circ F_{\Delta t_2} \\ &= g \circ F_{\Delta t_1 + \Delta t_2}. \end{aligned} \quad (9)$$

The semi-group property has many connections with recurrence processes [34] as the sequential observables can be predicted by repeatedly applying the Koopman operator $\mathcal{K}_{\Delta t}$. The core idea behind this point is similar to recurrence neural networks. When the Koopman operator is lifted to the product space of $\mathcal{H}(\mathcal{S}, \mathcal{A})$, it will become a controlled dynamical system beyond the prediction; then it can recurrently execute the feedback control by MPC.

- (Equivariant structure induced by group action g) The Koopman operator has a good representation of original space $\mathcal{S} \times \mathcal{A}$; the operator $\mathcal{K}_{\Delta t}$ can be regarded as an equivariant form as the forward dynamics $F_{\Delta t}$. When $g \in G$ is a group action $\rho : G \times (\mathcal{S}, \mathcal{A}) \rightarrow \mathcal{H}(\mathcal{S}, \mathcal{A})$ (similar to the idea in Equation (5)), it is easy to derive that

$$F_{\Delta t} = g^{-1}\mathcal{K}_{\Delta t}g,$$

where it can assert the equivariant relationship between $F_{\Delta t}$ and $\mathcal{K}_{\Delta t}$, and g can be regarded as a representation of the space induced by $\mathcal{S} \times \mathcal{A}$.

The time derivative of the observable $g \in \mathcal{C}^1$ can be represented as:

$$\dot{g} = \lim_{\Delta t \rightarrow 0} \frac{\mathcal{K}_{\Delta t}g - g}{\Delta t} = \lim_{\Delta t \rightarrow 0} \frac{g \circ F_{\Delta t} - g}{\Delta t} = Pg, \quad (10)$$

where \dot{g} is the derivative of $\mathcal{H}(\mathcal{S}, \mathcal{A})$ w.r.t. time t . The operator P defined on observables is the 1-order differentiation action, which can be analogous to the Gâteaux derivative [35]. Equation (10) has many connections with the geometric representation of the dynamical system. In this paper, instead of learning a model for data augmentation in the conventional framework, we will lift ² the differential dynamical system to an equivariant geometry by Pg . Therefore, Pg can be regarded as the tangent space of induced Koopman geometry. In the next subsection, an interpretation of the geometry from the Koopman operator will be given from the perspective of Lie algebra (see details in Appendix B).

¹Semi-group is an algebraic structure (G, \cdot) with the property of associativity.

²Lift has a two-fold meaning in this paper. Firstly, we extend the uncontrolled dynamical system to controlled dynamics such that $s \rightarrow f(s, a)$. For the Koopman operator, the uncontrolled dynamics are lifted to the controlled dynamics as $s_T \mapsto \mathcal{K}_{\Delta t}(s_T, a_T)$. The second-fold meaning is lifting the tangent information of the original manifold to the Lie group (equivariant geometry) such that $s_T \mapsto Pg(s_T) \in TG$.

3.2 Learning the Koopman Equivariant Geometry and Lifted Operators

To learn the differential form of the equivariant geometry, one must ensure the diffeomorphism between the equivariant geometry and the original geometry. To this end, this research proposes a decomposable form of dynamical systems (intrinsic autonomous dynamical system with extrinsic controller) through a diffeomorphic representation given by the following lemma. It should be noted that the *observable*, *latent* and *spectral* spaces all indicate the g -induced space³.

Lemma 1. (Diffeomorphic representation of decomposable dynamical systems) When the controlled dynamical system is decomposable, it satisfies the following form:

$$\dot{s} = \underbrace{f(s) + B(s)a}_{=f(s,a)}. \quad (11)$$

As the diffeomorphic property holds for the Koopman operator, the dynamical system in the equivariant geometry can be represented in the following form:

$$\dot{z}_t = \underbrace{Pz_t}_{\text{intrinsic tangent field}} + \underbrace{\tilde{B}(z_t)a_t}_{\text{diffeomorphism of controller}}, \quad (12)$$

where $z_t = g(s_t)$, $s_t \in \mathcal{S}$ is the state and \dot{z}_t is the curve derivative w.r.t t . In Equation (12), Pz_t is the intrinsic tangent field, and $\tilde{B}(z_t)$ is lifted from $B(s)$ only related to the design of the controller.

Remark 2. Where z_t without interventions of action a can be regarded as an equivariant geometry from the g -transformation of the original autonomous dynamical system, and Pz_t is the intrinsic tangent field. The product space of $\mathcal{H}(\mathcal{S}, \mathcal{A})$ lifts the autonomous dynamical system to the controlled ones. Under the diffeomorphism property (f -linear property [36]), the $(g_*B)(s_t)$ is the pushforward of the controller operator⁴, then $\tilde{B}(z)$ is the lifted from of $B(s)$ defined on the left-hand side of action a . For short, we will denote the $\mathcal{H}(\mathcal{S}, \mathcal{A})$ as \mathcal{H} .

Remark 3. The diffeomorphism provided by the map g serves as a tool for deriving the differential 1-form within the equivariant geometry (see Equation (12)). This transformation enables the linearization of complex problems locally within the equivariant geometry, allowing us to utilize the vector field information to obtain an analytical representation of the lifted policy in the later section.

In this research, similar to [32, 28], the auto-encoder neural network is used to learn the finite approximation of the introduced Koopman geometry under g -transformation. The encoder and decoder pairs are denoted as $g^{\text{en}}: \mathcal{S} \mapsto \mathcal{H}$ and $g^{\text{de}}: \mathcal{H} \mapsto \mathcal{S}$, respectively, such that $g^{\text{en}} \circ g^{\text{de}} = \text{Id}$. Here, the property preserves the isomorphism under the adjoint map such that $s_t = \text{Ad}_g(z_t)$ (a morphism diagram is shown in Appendix B). Given a sequence of state $\mathbf{s}_{T:T+(N-1)\Delta t} = \{s_T, \dots, s_{T+(N-1)\Delta t}\}$ from time T ⁵ to $T + (N - 1)\Delta t$ with a 1-step shift sequence $\mathbf{s}_{T+\Delta t:N\Delta t} = \{s_{T+\Delta t}, \dots, s_{T+N\Delta t}\}$, the two sequences are firstly transformed into the equivariant geometry by the encoder as $g^{\text{en}}(\mathbf{s}_{T:T+(N-1)\Delta t}) = \mathbf{z}_{T:T+(N-1)\Delta t} = \{z_T, \dots, z_{T+(N-1)\Delta t}\}$. Then the two operators P and \tilde{B} can be approximated with the applied action sequence $\mathbf{a}_{T:T+(N-1)\Delta t} = \{a_T, \dots, a_{T+(N-1)\Delta t}\}$ by

$$\hat{P}, \hat{\tilde{B}} = \arg \min_{P, \tilde{B}} \underbrace{\| \mathbf{z}_{T:T+(N-1)\Delta t} + \underbrace{[P\mathbf{z}_{T:T+(N-1)\Delta t} + \tilde{B}(\mathbf{z}_{T:T+(N-1)\Delta t})\mathbf{a}_{T:T+(N-1)\Delta t}]\Delta t}_{\text{Eluer Step}} - \mathbf{z}_{T+\Delta t:N\Delta t} \|_2}_{\text{approximation of } \dot{\mathbf{z}}_{T+\Delta t:N\Delta t}}, \quad (13)$$

where $\hat{P} \in \mathbb{R}^{d \times d}$, $\hat{\tilde{B}} \in \mathbb{R}^{d \times m \times d}$ and $z \in \mathbb{R}^d$. Intuitively, the approximated matrix \hat{P} can be understood as a Jacobian matrix over latent space. The tensor $\hat{\tilde{B}}$ plays the role of an extrinsic derivative operator, acting along the equivariant geometry, and can be associated with the left-side action operator.

³The various concepts of the g -induced space become clearer when considered in different contexts. The original paper [18] refers to the states after g -transformation as observables. In the context of E2C, the latent transformation action from the original space to the latent space aligns closely with the essence of g . In the KEEC framework, we employ g as the diffeomorphic function responsible for mapping the original manifold dynamical system to a Lie group. This Lie group not only functions as a smooth manifold but also possesses properties derived from Hilbert space. Therefore, the geometry-related definition in our context is more specific than the observables and latent spaces.

⁴We have indicated the diffeomorphic map $g: M \rightarrow G$ see Appendix B, the pushforward $g_*: TM \rightarrow TG$ helps to calculate the tangent information on the equivariant geometry.

⁵ T can be an arbitrary real value and $\Delta t \ll 1$.

Learning the Koopman equivariant geometry. To learn the desired pushforward auto-encoder ⁶ (See Equation (28) in Appendix C.1), which satisfies the diffeomorphic property, three losses are used to train the encoder and decoder in total.

- **Forward Loss** consists of two losses where the first loss is the auto-encoder loss, working as the isomorphic constraint. The second loss is the predication loss, correcting the integral curve over the equivariant geometry. By combining the two terms, the loss function can be obtained as

$$\mathcal{E}_{\text{fwd}} = \sum_{\tau=T}^{T+(N-1)\Delta t} \underbrace{\|g^{\text{de}}(\hat{z}_{\tau+\Delta t}) - g^{\text{de}}(z_{\tau+\Delta t})\|}_{\text{Integral Flow Correction}} + \underbrace{\|g^{\text{de}} \circ g^{\text{en}}(s_{\tau}) - s_{\tau}\|}_{\text{Isomorphic Constraint}}, \quad (14)$$

where $z_{\tau+\Delta t} = g^{\text{en}}(s_{\tau+\Delta t})$ and $\hat{z}_{\tau+\Delta t} = z_{\tau} + [\hat{P}z_{\tau} + \hat{B}(z_{\tau})a_{\tau}]\Delta t$. The analytical solution to the least square regression problem (13) is used to calculate \hat{P} and \hat{B} , which does not require explicitly optimizing two tensors and stabilize the training iteration. Notably, the decoder g^{de} was introduced only for imposing the constraints for the encoder. In the following control task, all the operations will be performed in the latent space, and the decoder is no longer needed in a *decoder-free* way. The part of *Integral Flow Correction* in the loss function is to correct the curve by the Euler step as the $\Delta t \ll 1$. The isomorphic constraint keeps the bijective relationship between the original manifold and equivariant geometry.

- **Isometric Loss** was imposed to preserve the distance in the original state space. The loss is defined as the absolute error between the distances measured in the equivariant geometry and that in the original manifold such that,

$$\mathcal{E}_{\text{metric}} = \sum_{\tau=T}^{T+(N-1)\Delta t} \left| \underbrace{\|z_{\tau+\Delta t} - z_{\tau}\|}_{\text{distance on equivariant geometry}} - \underbrace{\|s_{\tau+\Delta t} - s_{\tau}\|}_{\text{distance on original manifold}} \right|, \quad (15)$$

This ensures the pointwise convergence of the Riemannian metric between the original manifold and equivariant geometry. The loss function, in this context, approximates the geodesic using 1–order differential information, known as the *locally linear property* ⁷. Without the isometric constraint, the induced Koopman geometry transforms into a *non-metrizable* space ⁸, breaking the assumption (a) of the continuum of control dynamics. Additionally, the invariant metric information preserves the compactness of the Koopman geometry, maintaining non-distortion. Notably, no other paper utilizing the Koopman operator mentions the isometric constraint. Even if the prediction of the next state is accurate, the encoding information becomes non-continuous in the latent space, violating the fundamental assumption of a Hamiltonian dynamical system. In such a scenario, controlling the dynamics over a distorted geometry in such a scenario becomes impractical. A comparison figure can be found in Figure 1, and more details will be given in Section 4.1.

The final training loss is the combination of the forward loss and isometric loss:

$$\mathcal{E} = \mathcal{E}_{\text{fwd}} + \lambda \mathcal{E}_{\text{metric}}. \quad (16)$$

The loss is minimized by optimizing the parameters in the pushforward auto-encoder $g^{\text{en}}, g^{\text{de}}$ using the stochastic gradient descent method. The trained encoder would be used solely to control the dynamics with the approximated lifted operators \hat{P}, \hat{B} , but can also be used in other downstream tasks such as future predication and system identification jointly with the trained decoder.

3.3 Equivariant Optimal Control

In this subsection, an equivariant value function will be established and approximated in the equivariant geometry instead of the original manifold. Unlike conventional Q-learning, we propose embedding the diffeomorphic dynamics to control without transferring to the original manifold. After obtaining the 1-order differentiation information, it can derive an analytic form of optimal action by diffeomorphic dynamics on the equivariant value equation.

Bellman Optimality on Equivariant Value Function. The value function approximation in the MPC control framework is considered in this context. Based on the original work [39], the N –step look-forward value function can be represented as

$$B^* \tilde{V}^k(s_T) = \max_{a_{T:T+(N-1)\Delta t}} \sum_{\tau=T}^{T+(N-1)\Delta t} \gamma^{\tau-T} (s_{\tau}, a_{\tau}) + \gamma^N \tilde{V}^k(s_{T+N\Delta t}), \quad \forall s_T \in S, \quad (17)$$

⁶The g -transformation is represented by a neural network as its universal approximation property for invariant maps [37].

⁷The geodesic error is $\mathcal{O}(\Delta t^2)$ when employing 1–order differential information.

⁸Metrizable space is a topological space that is homeomorphic to a metric space [38].

where B^* is the Bellman operator and $k + 1, k \in \mathbb{N}^+$ are the iteration times of the approximated value function \tilde{V} . It is well-known that the approximated value function will contract to the fixed point [40, 41], such that

$$\limsup_{k \rightarrow \infty} \|\tilde{V}^k - V^*\|_\infty \leq \epsilon,$$

where V^* is the optimal value function and ϵ is arbitrary small. Identifying the greedy action involves evaluating all conceivable actions when dealing with discrete actions. However, exploring continuous action spaces poses a technical challenge due to the infinite number of possible actions. Conversely, discretizing these spaces leads to exponential growth of computational complexity with the increasing number of states and actions. To solve this problem, the equivariant value function can significantly improve the computational efficiency due to the discretization invariance of the Koopman operator. Instead of solving the problem in the original manifold, the approximated value function in the equivariant geometry is equivalent to the original one. For simplicity, the value function defined on the equivariant geometry is denoted as V_g , it can be represented as

$$B^* \tilde{V}_g^k(z_t) = \max_{a_t} r_g(z_t) + \gamma \tilde{V}_g^k(\mathcal{K}_{\Delta t}(z_t); \theta), \quad (18)$$

where $z_t = g(s_t)$, r_g is the reward function defined on equivariant geometry, and the optimization problem becomes:

$$\theta^{k+1} = \arg \min_{z \in \mathcal{D}} \|B^* V_g(z_t) - \tilde{V}_g^k(z_t; \theta)\|, \quad (19)$$

where $\tilde{V}(z, \theta)$ is the approximated value function, θ^{k+1} is the parameters in $(k + 1)$ -iteration and \mathcal{D} is the dataset. Theorem 1 is proposed to guarantee the equivalence of value functions defined on equivariant geometry and the original manifold such as $V_g \sim V$.

Theorem 1. (Equivariance of Value Function). The dynamical system is g -invariant under the Koopman representation; then the value function $V^\pi(s) = V_g^\pi(z)$ for any state $s \in \mathcal{S}$ and policy $\pi \in \Pi$.

See detailed proof in Appendix C.2.

Remark 4. The equivariance of the value function can be directly proven from a group representation perspective in Hilbert space. Generally, the corresponding spectral decomposition induces a Reproducing Kernel Hilbert Space (RKHS), and the Koopman-induced equivariant value function will be equal to the original value function almost everywhere according to the reproducing property in RKHS.

Remark 5. According to Lemma 1 and Theorem 2, the control of the equivariant geometry can achieve the invariant effect compared to the original manifold. The lifted 1-differential form information can directly derive the optimal action π^* in equivariant geometry instead of the original manifold.

Analytical Form of Lifted Policy. For the typical RL, the approximated value function is solved by Q -learning, which is inefficient [28, 42]. This is because when computing the value function target, it would need to solve an exponentially large discrete optimization problem in each iteration. To improve the computation efficiency, the differential information on the Koopman-induced equivariant geometry will provide an analytical-form solution instead of solving a discrete optimization problem.

Theorem 2. (Analytical form of lifted policy on equivariant geometry). When the Lemma 1 holds, the optimal policy for the value function in the equivariant geometry has the closed-form solution as

$$\pi^*(z_t) = -[\nabla \langle R_1, \cdot \rangle]^\dagger (\gamma \nabla_z V_g^T \cdot \tilde{B}(z)), \Delta t \quad (20)$$

where R_1 (determined by reward function in the RL environment) is the functional defined on the dual space of action \mathcal{A} , $\nabla \langle R_1, \cdot \rangle$ is a square matrix and Δt is the time interval of each step. Here, V_g is assumed to be a convex function. If the reward has a quadratic form, the optimal action can be written as

$$\pi^*(z_t) = -\gamma R_1^\dagger [z_t^T M(z_t) + \frac{1}{2} \gamma (z_t - z^*)^T \frac{\partial M(z_t)}{\partial z} (z_t - z^*)] \tilde{B}(z_t), \quad (21)$$

where $V_g(z) = -z^T M(z)z + b$, $M(z)$ is positive definite and b is a constant. The main text omitted the proof, and the detailed proof is given in Appendix C.3.

Remark 6. The proof of the theorem is directly developed from the dynamic programming [40] and the Hamilton-Jacobi-Bellman (HJB) equation [43]. Our method significantly differs from the search for an optimal action in tabular-Q learning [28]. The analytical form of optimal action is directly performed on a continuum by learned diffeomorphic dynamics (12). The optimal policy will be invariant since the equivariant value function on equivariant geometry is

equivalent to the original manifold. Beyond the computational efficiency, the convergence of $\tilde{V}_g(\theta)$ can achieve a fast convergence rate to V^{π^*} , which will be indicated as the following theorem.

Theorem 3. (Quadratic Convergence of The Equivariant Value Function). When Theorem 1 and 2 hold, the approximated value function will point-wisely converge to the optimal value function, and the convergence rate is quadratic as

$$\|\tilde{V}_g^{k+1} - V_g^{\pi^*}\| = \mathcal{O}(\|\tilde{V}_g^k - V_g^{\pi^*}\|^2), \quad (22)$$

where approximated value function $\tilde{V}_g(\theta)$ is dependent on the parameters θ , the updating \tilde{V}_g^{k+1} is updated as shown in Equation (19). The detailed proof and description of the geometric understanding of Theorem 3 is given in Appendix C.4.

Remark 7. The proof of the quadratic convergence rate can be analogous to Newton’s step. The fact significantly differs from the actor-critic RL methods, where the policy π needs to be updated incrementally. The conventional RL relies on asynchronous updating of value function and policy, which causes a low convergence rate [44]. This paper’s analytical form of optimal policy provides a ‘momentum’ to boost the convergence rate. In the detailed proof, the convergence of the equivariant value function $\{\tilde{V}_g(\theta^k)\}_{k=1}^{\infty}$ is treated as a Cauchy net in the functional space contracting to the fixed point $V_g^{\pi^*}$. The proof has a natural connection to Newton-Raphson method [45], and a geometric interpretation is given in the cases of this research.

Learning the Equivariant Value Function. Based on the analytical form of optimal policy derived in Equation (20) and (21), the equivariant value function can be updated as in Equation (19). The loss function can be represented as

$$\mathcal{E}_{\text{evf}} = \sum \|V_g(z_t, \theta) - \underbrace{(r_g(z_t, a^*) + \gamma \tilde{V}_g^k(\mathcal{K}_{\Delta t}(z_t), \theta))}_{\text{one-step rollout}}\|, \quad (23)$$

where $a^* = \pi^*(z_t) = -[\nabla \langle R_1, \cdot \rangle]^\dagger (\gamma \nabla_z V_g^T \cdot \tilde{B}(z)) \Delta t$ derived in Equation (20). In some situations, the equivariant value function can be set as a quadratic form as $V_g(z, \theta) = -z^T M(z, \theta) z + b(\theta)$, the optimal action in the Equation (23) becomes $a^* = -\gamma R_1^\dagger [z_t^T M(z_t) + \frac{1}{2} \gamma (z_t - z^*)^T \frac{\partial M(z_t)}{\partial z} (z_t - z^*)]$.

At the end of Section 3, our KEEC can be decomposed into two steps:

1. Training the auto-encoder as the approximation for Koopman embedding and estimating the lifted operators P, B .
2. Bellman iteration with trained Koopman dynamics model for training the equivariant value function. The details are summarized in the Algorithm 1.

Algorithm 1 KEEC: Koopman Embedding to Equivariant Control

Require: random control trajectories $\mathcal{D} = \{\mathcal{T}_\tau\}_{\tau=T}^{T+N\Delta t}$ where $\mathcal{T}_\tau = (s_\tau, a_\tau, r_\tau)$, auto-encoder $g_\psi^{\text{en}}, g_\phi^{\text{de}}$, value net $\tilde{V}_g(\cdot, \theta)$, learning rate α

- 1: **for** iteration n **do** ▷ Train Koopman Embedding
- 2: Approximate operators \hat{P} and \hat{B} by minimizing Equation (13) with current $g_{\psi^n}^{\text{en}}, g_{\phi^n}^{\text{de}}$
- 3: Update auto-encoder $\psi^{n+1}, \phi^{n+1} = \psi^n + \alpha \nabla_\psi \mathcal{E}, \phi^n + \alpha \nabla_\phi \mathcal{E}$ where \mathcal{E} in Equation (16)
- 4: **end for**
- 5: **for** iteration n **do** ▷ Train Value Function
- 6: Update value net $\theta^{n+1} = \theta^n + \alpha \nabla_\theta \mathcal{E}_{\text{evf}}$ with trained encoder g_ψ^{en} where \mathcal{E}_{evf} in Equation (23)
- 7: **end for**
- 8: **return** encoder g_ψ^{en} , value net $\tilde{V}_g(\cdot, \theta)$

4 Experiments

The proposed KEEC is evaluated through its ability to control various dynamical systems to their optimal state, i.e. an unstable steady state, including the Swing-up Pendulum and Lorenz-63 stabilization tasks.

Baselines. This research benchmarked KEEC against three different algorithms. As a model-based approach, it compares KEEC with the informatic variant of the Model Predictive Path Integral (MPPI) algorithm [46]. The MPPI algorithm trained multi-layer neural networks as the dynamics model and then derived optimal control as an importance-weighted average over sampled trajectories from the trained dynamics model that approximates the optimal control

input distribution. Additionally, it also compares with two other model-free algorithms: Soft Actor-Critic (SAC) [47] represents the benchmark in online RL, and Conservative Q-Learning (CQL) [48], which is a notable approach in offline RL. The benchmarked algorithms encompass model-based, online model-free, and offline model-free RL approaches, providing a comprehensive investigation of the effectiveness of KEEC. The model parameters and architecture details are in the Appendix D.

Data Generation. For offline algorithms (KEEC, CQL, and MPPI), 50,000 episodes are generated for Pendulum and Lorenz-63, respectively. 90% of them are used for training, and the rest for testing. Each episode has 50-time steps with random actions, random initials, and recording the rewards. The rewards are designed as a negative quadratic cost, such that $r(s_i, a_i) = -(\|s_i - s^*\|_2 + \lambda_{\text{cost}}\|a_i\|_2)$, where action penalty coefficient $\lambda_{\text{cost}} = 0.01$ for all the tasks and s^* is the specified optimal state. The data are generated by integration using the 4th order Runge-Kutta with a time step $\Delta t = 0.05$ and $\Delta t = 0.1$ for Pendulum and Lorenz-63, respectively. For constructing the dataset, we slice the sampled trajectories w.r.t. multi-steps $N = 8$ for KEEC and single step $N = 1$ for CQL and MPPI such that $D_{\text{in}} = \{s_\tau, a_\tau\}_{\tau=T}^{T+(N-1)\Delta t}$ and $D_{\text{out}} = \{s_\tau\}_{\tau=T}^{T+N\Delta t}$, and then shuffle all the sliced data. For the online algorithm (SAC), the SAC algorithm runs interacting with the environments with 5,000 episodes where each episode has 500 time steps, and the number of single steps is the same as the offline data.

Training and Evaluation Metric. All models are trained using Adam optimizer [49] with a decaying learning rate initially set to 0.001. For KEEC, 50 training epochs are used for system identification with a batch size of 32, and 20 training epochs for learning the value function with a batch size of 256. The dimensions of latent geometry in both the Swing-up pendulum and Lorenz-63 stabilization are set to be $d = 32$. The loss weights are set to $\lambda = 0.3$ in Equation (16) for the isometric constraint $\mathcal{E}_{\text{metric}}$. For the two offline models, 70 epochs were applied to train the models with a batch size of 256. The model parameters for the online SAC were updated per 10 steps with batch size 256 and enhanced with a replay-memory buffer of 100k. This results in 250k iterations of gradient steps. The training settings above are the same for the Swing-up pendulum and Lorenz-63. The average and standard deviation of episodic reward is used as the evaluation criteria to measure the control performance and robustness. All other hyperparameters are the same as proposed in the respective papers.

Table 1: Summary of results for the Swing-up pendulum and Lorenz63 stabilization task. The results are the mean and standard deviation of 100 random initial states with time intervals $N = 500$ and 5000.

Algorithm	Task	Episodic Reward					Time Step	Online Policy
		Min	Max	Avg	Std			
SAC	Pendulum	-144.23	-1.39	-95.27	48.67	0.5k	✓	
CQL	Pendulum	-178.91	-2.86	-128.23	76.94	0.5k	✗	
MPPI	Pendulum	-233.67	-5.69	-187.20	78.72	0.5k	✗	
KEEC	Pendulum	-157.35	-1.12	-97.88	44.96	0.5k	✗	
KEEC (w/o $\mathcal{E}_{\text{metric}}$)	Pendulum	-3.7k	-2.5k	-3.3k	228.72	0.5k	✗	
SAC	Lorenz-63	-75.4k	-3.2k	-44.9k	13.7k	5.0k	✓	
CQL	Lorenz-63	-102.8k	-56.4k	-81.2k	9.2k	5.0k	✗	
MPPI	Lorenz-63	-118.1k	-75.7k	-87.6k	18.3k	5.0k	✗	
KEEC	Lorenz-63	-69.1k	-1.1k	-25.3k	11.2k	5.0k	✗	
KEEC (w/o $\mathcal{E}_{\text{metric}}$)	Lorenz-63	-97.8k	-55.9k	-83.5k	17.2k	5.0k	✗	

4.1 Swing-up Pendulum

The Swing-up pendulum problem is a classic control problem that involves a pendulum starting from a downward, hanging position and swinging it up to its unstable, inverted position. This problem is challenging due to the pendulum’s nonlinear dynamics and the need to stabilize it at the unstable saddle point (i.e., the upright position). The problem has 2 state dimensions: angular θ and angular velocity $\dot{\theta}$ with the equation of pendulum motion:

$$\frac{d^2\theta}{dt^2} = \frac{3g}{2l} \sin\theta + \frac{3}{ml^2}a, \quad (24)$$

where l is the length of the pendulum with a mass m , g is the gravitational acceleration, and a is the applied torque, acting as the control input. The common choices with $m = 1, l = 1, g = 10$, and $a \in [-2, 2]$ were taken in this research.

Figure 1 demonstrates the impact of incorporating the isometric constraint $\mathcal{E}_{\text{metric}}$ in learning the equivariant geometry and equivariant value function V_g . To visualize the high-dimensional equivariant geometry, we use the Locally Linear Embedding (LLE) [50], which is an unsupervised learning algorithm that computes a low-dimensional and metric-preserving representation of high-dimensional objects, to project the equivariant geometry from $d = 32$ to 3 (see Figure

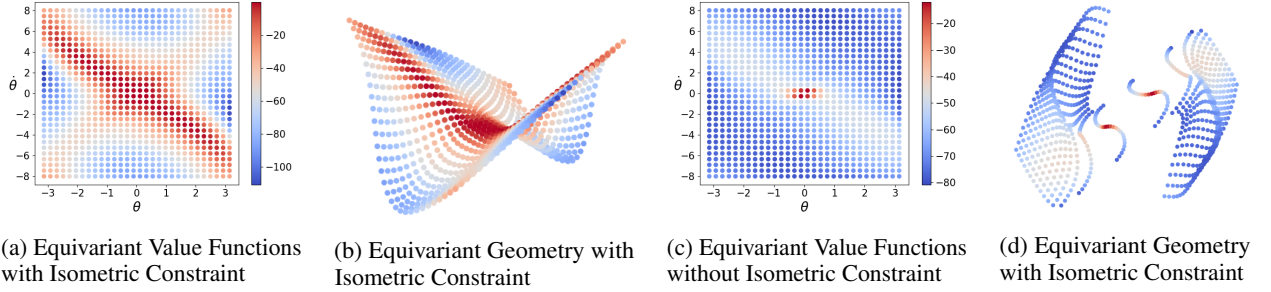


Figure 1: Comparison of learned equivariant value functions and equivariant geometries with/without the isometric constraint in Swing-up Pendulum task. The varying colours of the points on original coordinates and learned geometries indicate the magnitude of the equivariant value function. The learned geometries are visualized through Locally Linear Embedding (LLE) [50] with a projection from dimension $d = 32$ to 3.

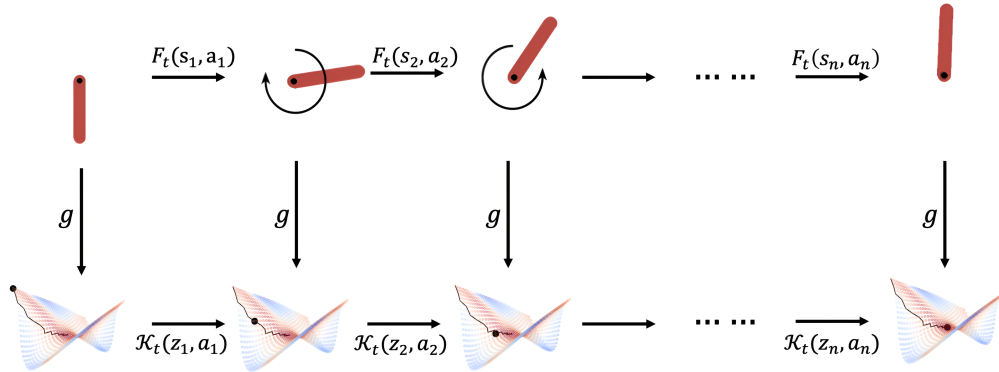


Figure 2: The Swing-up Pendulum control task aims to stabilize the pendulum in an unstable inverted position, initiating from the state $(\theta = \pi, \dot{\theta} = -8)$. The black line is the corresponding moving trajectory of the pendulum, while the black dot signifies the pendulum’s real-time position.

1b and 1d). Including the isometric constraint ensures that the metric of the original space is preserved in the learned geometry, as shown in Figure 1b. The shape of the learned geometry can typically represent a classic Hamiltonian dynamical system. Another key observation is that the saddle point in the equivariant geometry, indicative of the optimal state, aligns with the inverted position in the pendulum system, characterized by reaching maximal potential energy and minimal kinetic energy. In contrast, the absence of the isometric constraint leads to notable distortions and non-compactness in the learned geometry, as clearly visible in Figure 1d. This distortion leads to discontinuities in the dynamical system, and more seriously, the saddle point will become unobservable. The practical implication of this observation is significant. When an initial point is chosen arbitrarily on the equivariant geometry, it is ideally transported along the most efficient path to the saddle point. However, if the equivariant value function is not defined on a continuum, the derivative information, which is crucial for directing the action as per Equation (20), becomes impossible. This highlights the importance of maintaining continuity and the intrinsic geometric properties in the equivariant geometry for successful control.

Figure 2 provides a visualization of the control process of the proposed KEEC. This figure shows a controlled trajectory from the initial point $(\theta = \pi, \dot{\theta} = -8)$ to the inverted position $(\theta = 0, \dot{\theta} = 0)$ from both original space and equivariant geometry. It is worth noting that the trajectory of the stabilized pendulum in the original space has a bijective relationship with the equivariant geometry. The pendulum’s motion is uniquely characterized as a path (black line) over the equivariant geometry, while the black points indicate the real-time corresponding position of the pendulum on the equivariant geometry. The quantitative results of the Swing-up Pendulum are shown in Table 1, where the statistics are a summary of the accumulated rewards for each episode for the time range $T = 500$. In general, KEEC significantly outperforms the two offline benchmarks, CQL and MPPI, regarding high reward and low variance. Although the average episodic reward of KEEC is slightly lower than SAC, it is still comparable with a smaller variance. The superior performance of SAC can be attributed to its online learning property. Figure 3 (left) shows 4 example KEEC control trajectories, and 3 (middle, right) demonstrates the means of control trajectories over 100 random initial states where the shaded area indicates the ± 1 standard deviations. In the Swing-up Pendulum task, our KEEC swings up the pendulum

after 50 steps on average and can robustly stabilize it in the upright position. However, failed controls of KEEC can be observed without the isometric constraint. SAC achieves a similar control performance as ours, whereas CQL can also achieve robust stabilization but requires 50 more steps to swing up the pendulum.

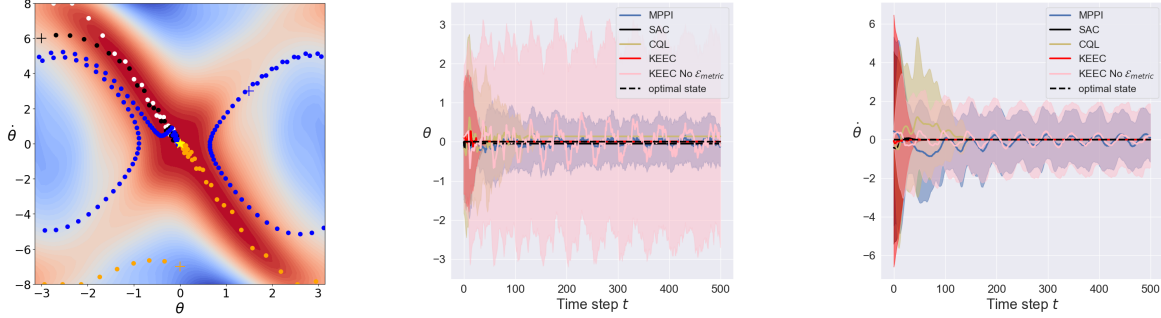


Figure 3: (Left) Example Control trajectories of KEEC with four random initials, where + indicates the initial points and the yellow star indicates the optimal state. (Middle, Right) The comparison of means and standard deviations of control trajectories in each dimension ($\theta, \dot{\theta}$) with 100 initials and time horizon $T = 500$

4.2 Lorenz-63

Next, this research considers the task of applying an affine control signal to each coordinate to control the Lorenz-63 model, which can be expressed as:

$$\begin{aligned}\frac{dx}{dt} &= \sigma(y - x) + v_x \\ \frac{dy}{dt} &= x(\rho - z) - y + v_y \\ \frac{dz}{dt} &= xy - \beta z + v_z,\end{aligned}$$

where $\mathbf{v} = (v_x, v_y, v_z) \in [-3, 3]^3$ is the applied control signal. The parameters $\sigma = 10$, $\rho = 28$, and $\beta = 8/3$ were chosen and exhibit chaotic behaviour with two strange attractors ($\pm\sqrt{\beta(\rho-1)}, \pm\sqrt{\beta(\rho-1)}, \rho-1$). The environmental state consists of (x, y, z) . This task aims to stabilise the environmental states at one of its strange attractors (8.5, 8.5, 27). Although the state will autonomously move towards the two strange attractors, stabilizing the system is not trivial because of its fractal oscillation and high sensitivity to a small perturbation inherited from its chaotic property. Figure 4 shows the trajectories of the uncontrolled and KEEC-controlled Lorenz-63 systems.

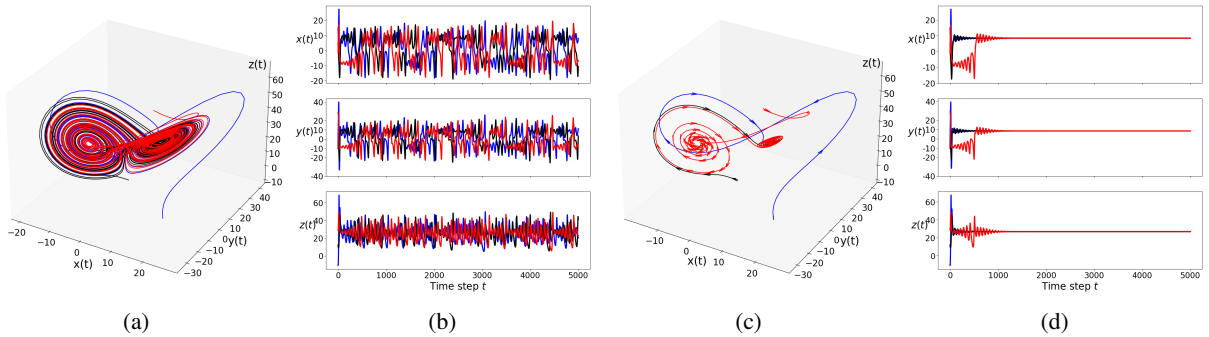


Figure 4: (a) and (c) uncontrolled and KEEC controlled 3d phase trajectories of Lorenz-63, where the arrows in (c) indicate the moving direction. (b) and (d) uncontrolled and controlled state trajectories of Lorenz-63.

The experimental results are summarized in Table 1. KEEC outperforms all three baseline models in terms of episodic rewards. The relatively large standard deviation can be attributed to some initial points far from the attractor, which takes more steps back and should not be a concern as KEEC also shows the best performance in the worst scenario. Figure 5 demonstrates control trajectories' mean and standard deviation over 100 random initial states. The KEEC can robustly stabilize the system after 3000 steps on average, which consistently outperforms the other three baselines. The

CQL and MPPI mostly failed to achieve stabilization, which can be observed from the departure of control trajectories from the attractor location and high oscillation (i.e., large shaded areas). The SAC is the most comparable approach to KEEC in this task, but the performance gap is still evident.

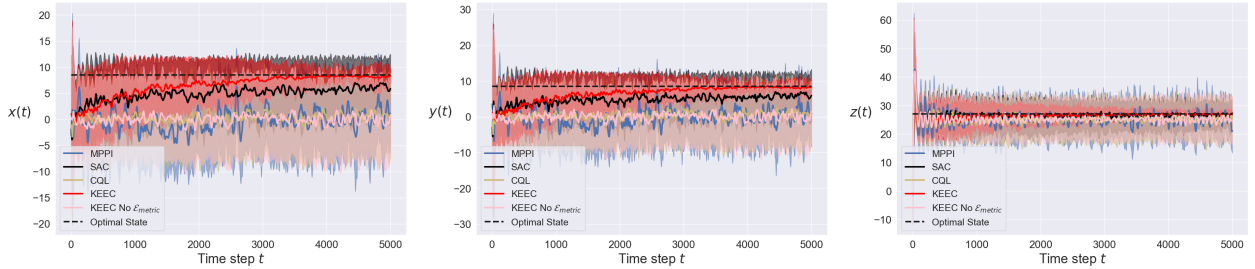


Figure 5: The comparison of mean and standard deviation of control trajectories in each state ($x(t)$, $y(t)$, $z(t)$, left to right) with 100 initial points and time horizon $T = 5000$.

5 Conclusion

This paper introduces KEEC, a novel control framework designed to tackle nonlinear control problems without explicit dynamical system models. KEEC achieves optimal control by learning an equivariant geometry under the Koopman operator, directly operating on this geometry instead of the original dynamical system. Additionally, KEEC provides a theoretical perspective on leveraging symmetric and equivariant representations to attain an invariant effect consistent with the original space. The discovery of differential information on the equivariant geometry enables the derivation of an analytical form, leading to the quadratic convergence of the equivariant value function. Experiments involving the pendulum and Lorenz-63 showcase the superior performance of KEEC compared to benchmarks in reinforcement learning algorithms such as SAC, CQL, and MPPI regarding both rewards and robustness.

The following three research directions are considered promising. Firstly, since KEEC is constructed as an operator by extracting physical information from geometry, extending it to few-shot scenarios seems plausible, especially for the conservation laws in dynamical systems [51] and the similarity of many Hamiltonian dynamics to symplectic manifold structures [52]. Secondly, considering the natural connections between the Koopman operator and the neural operator theory [33], there is potential for extending the Koopman operator to control real-world complex dynamical systems, such as fluids [53] and plasma [54]. Finally, the paper highlights the significant improvement in encoding symmetric differential information for complex control problems. Thus, a promising avenue for future research lies in combining neural operator theory with symmetry representation for enhanced control strategies.

References

- [1] M. Zhang, S. Vikram, L. Smith, P. Abbeel, M. Johnson, and S. Levine, “Solar: Deep structured representations for model-based reinforcement learning,” in *International conference on machine learning*, pp. 7444–7453, PMLR, 2019.
- [2] A. X. Lee, A. Nagabandi, P. Abbeel, and S. Levine, “Stochastic latent actor-critic: Deep reinforcement learning with a latent variable model,” *Advances in Neural Information Processing Systems*, vol. 33, pp. 741–752, 2020.
- [3] M. Watter, J. Springenberg, J. Boedecker, and M. Riedmiller, “Embed to control: A locally linear latent dynamics model for control from raw images,” *Advances in neural information processing systems*, vol. 28, 2015.
- [4] Y. D. Zhong, B. Dey, and A. Chakraborty, “Symplectic ode-net: Learning hamiltonian dynamics with control,” *arXiv preprint arXiv:1909.12077*, 2019.
- [5] K. Miao and K. Gatsis, “Learning robust state observers using neural odes,” in *Learning for Dynamics and Control Conference*, pp. 208–219, PMLR, 2023.
- [6] L. Kaiser, M. Babaeizadeh, P. Milos, B. Osinski, R. H. Campbell, K. Czechowski, D. Erhan, C. Finn, P. Kozakowski, S. Levine, *et al.*, “Model-based reinforcement learning for atari,” *arXiv preprint arXiv:1903.00374*, 2019.
- [7] A. V. Nair, V. Pong, M. Dalal, S. Bahl, S. Lin, and S. Levine, “Visual reinforcement learning with imagined goals,” *Advances in neural information processing systems*, vol. 31, 2018.
- [8] R. P. Adams and P. Orbanz, “Representing and learning functions invariant under crystallographic groups,” *arXiv preprint arXiv:2306.05261*, 2023.
- [9] B. Bloem-Reddy and Y. W. Teh, “Probabilistic symmetries and invariant neural networks,” *The Journal of Machine Learning Research*, vol. 21, no. 1, pp. 3535–3595, 2020.
- [10] M. M. Bronstein, J. Bruna, Y. LeCun, A. Szlam, and P. Vandergheynst, “Geometric deep learning: going beyond euclidean data,” *IEEE Signal Processing Magazine*, vol. 34, no. 4, pp. 18–42, 2017.
- [11] J. Y. Park, O. Biza, L. Zhao, J. W. van de Meent, and R. Walters, “Learning symmetric embeddings for equivariant world models,” *arXiv preprint arXiv:2204.11371*, 2022.
- [12] D. Wang, R. Walters, and R. Platt, “SO(2)-equivariant reinforcement learning,” in *International Conference on Learning Representations*, 2021.
- [13] S. Rezaei-Shoshtari, R. Zhao, P. Panangaden, D. Meger, and D. Precup, “Continuous mdp homomorphisms and homomorphic policy gradient,” *Advances in Neural Information Processing Systems*, vol. 35, pp. 20189–20204, 2022.
- [14] I. Higgins, D. Amos, D. Pfau, S. Racaniere, L. Matthey, D. Rezende, and A. Lerchner, “Towards a definition of disentangled representations,” *arXiv preprint arXiv:1812.02230*, 2018.
- [15] E. Van der Pol, D. Worrall, H. van Hoof, F. Oliehoek, and M. Welling, “Mdp homomorphic networks: Group symmetries in reinforcement learning,” *Advances in Neural Information Processing Systems*, vol. 33, pp. 4199–4210, 2020.
- [16] T. Miyato, M. Koyama, and K. Fukumizu, “Unsupervised learning of equivariant structure from sequences,” *Advances in Neural Information Processing Systems*, vol. 35, pp. 768–781, 2022.
- [17] M. Koyama, K. Fukumizu, K. Hayashi, and T. Miyato, “Neural fourier transform: A general approach to equivariant representation learning,” *arXiv preprint arXiv:2305.18484*, 2023.
- [18] B. O. Koopman, “Hamiltonian systems and transformation in hilbert space,” *Proceedings of the National Academy of Sciences*, vol. 17, no. 5, pp. 315–318, 1931.
- [19] B. O. Koopman and J. v. Neumann, “Dynamical systems of continuous spectra,” *Proceedings of the National Academy of Sciences*, vol. 18, no. 3, pp. 255–263, 1932.
- [20] M. O. Williams, I. G. Kevrekidis, and C. W. Rowley, “A data-driven approximation of the koopman operator: Extending dynamic mode decomposition,” *Journal of Nonlinear Science*, vol. 25, pp. 1307–1346, 2015.
- [21] N. Takeishi, Y. Kawahara, and T. Yairi, “Learning koopman invariant subspaces for dynamic mode decomposition,” *Advances in neural information processing systems*, vol. 30, 2017.

- [22] H. Arbabi and I. Mezić, “Ergodic theory, dynamic mode decomposition, and computation of spectral properties of the koopman operator,” *SIAM Journal on Applied Dynamical Systems*, vol. 16, no. 4, pp. 2096–2126, 2017.
- [23] D. Bruder, B. Gillespie, C. D. Remy, and R. Vasudevan, “Modeling and control of soft robots using the koopman operator and model predictive control,” *arXiv preprint arXiv:1902.02827*, 2019.
- [24] D. Bruder, C. D. Remy, and R. Vasudevan, “Nonlinear system identification of soft robot dynamics using koopman operator theory,” in *2019 International Conference on Robotics and Automation (ICRA)*, pp. 6244–6250, IEEE, 2019.
- [25] Y. Li, H. He, J. Wu, D. Katabi, and A. Torralba, “Learning compositional koopman operators for model-based control,” *arXiv preprint arXiv:1910.08264*, 2019.
- [26] J. Morton, A. Jameson, M. J. Kochenderfer, and F. Witherden, “Deep dynamical modeling and control of unsteady fluid flows,” *Advances in Neural Information Processing Systems*, vol. 31, 2018.
- [27] M. Korda and I. Mezić, “Linear predictors for nonlinear dynamical systems: Koopman operator meets model predictive control,” *Automatica*, vol. 93, pp. 149–160, 2018.
- [28] M. Weissenbacher, S. Sinha, A. Garg, and K. Yoshinobu, “Koopman Q-learning: Offline reinforcement learning via symmetries of dynamics,” in *International Conference on Machine Learning*, pp. 23645–23667, PMLR, 2022.
- [29] M. Okada and T. Taniguchi, “Variational inference mpc for bayesian model-based reinforcement learning,” in *Conference on robot learning*, pp. 258–272, PMLR, 2020.
- [30] M. Mittal, M. Gallieri, A. Quaglino, S. S. M. Salehian, and J. Koutník, “Neural lyapunov model predictive control: Learning safe global controllers from sub-optimal examples,” *arXiv preprint arXiv:2002.10451*, 2020.
- [31] D. Brandfonbrener and J. Bruna, “Geometric insights into the convergence of nonlinear td learning,” *arXiv preprint arXiv:1905.12185*, 2019.
- [32] A. Mauroy, Y. Susuki, and I. Mezić, *Koopman operator in systems and control*. Springer, 2020.
- [33] N. Kovachki, Z. Li, B. Liu, K. Azizzadenesheli, K. Bhattacharya, A. Stuart, and A. Anandkumar, “Neural operator: Learning maps between function spaces,” *arXiv preprint arXiv:2108.08481*, 2021.
- [34] O. Azencot, N. B. Erichson, V. Lin, and M. Mahoney, “Forecasting sequential data using consistent koopman autoencoders,” in *International Conference on Machine Learning*, pp. 475–485, PMLR, 2020.
- [35] J. Bell, “Fréchet derivatives and gâteaux derivatives,” *Department of Mathematics*, 2014.
- [36] H. W. Guggenheimer, *Differential geometry*. Courier Corporation, 2012.
- [37] D. Yarotsky, “Universal approximations of invariant maps by neural networks,” *Constructive Approximation*, vol. 55, no. 1, pp. 407–474, 2022.
- [38] G. Gruenhagen, “Metriizable spaces and generalizations,” *Recent Progress in General Topology II, Elsevier, Amsterdam*, pp. 201–225, 2002.
- [39] R. Bellman, “Dynamic programming,” *Science*, vol. 153, no. 3731, pp. 34–37, 1966.
- [40] D. Bertsekas, *Dynamic programming and optimal control: Volume I*, vol. 4. Athena scientific, 2012.
- [41] M. G. Lagoudakis and R. Parr, “Least-squares policy iteration,” *The Journal of Machine Learning Research*, vol. 4, pp. 1107–1149, 2003.
- [42] J. Du, J. Futoma, and F. Doshi-Velez, “Model-based reinforcement learning for semi-markov decision processes with neural odes,” *Advances in Neural Information Processing Systems*, vol. 33, pp. 19805–19816, 2020.
- [43] J. Yong and X. Y. Zhou, *Stochastic controls: Hamiltonian systems and HJB equations*, vol. 43. Springer Science & Business Media, 1999.
- [44] R. S. Sutton and A. G. Barto, *Reinforcement learning: An introduction*. MIT press, 2018.
- [45] S. J. Wright, *Numerical optimization*. Springer New York, NY, 2006.
- [46] G. Williams, N. Wagener, B. Goldfain, P. Drews, J. M. Rehg, B. Boots, and E. A. Theodorou, “Information theoretic mpc for model-based reinforcement learning,” in *2017 IEEE International Conference on Robotics and Automation (ICRA)*, pp. 1714–1721, IEEE, 2017.

- [47] T. Haarnoja, A. Zhou, P. Abbeel, and S. Levine, “Soft actor-critic: Off-policy maximum entropy deep reinforcement learning with a stochastic actor,” in *International conference on machine learning*, pp. 1861–1870, PMLR, 2018.
- [48] A. Kumar, A. Zhou, G. Tucker, and S. Levine, “Conservative q-learning for offline reinforcement learning,” *Advances in Neural Information Processing Systems*, vol. 33, pp. 1179–1191, 2020.
- [49] D. Kingma and J. Ba, “Adam: A method for stochastic optimization,” in *International Conference on Learning Representations (ICLR)*, (San Diego, CA, USA), 2015.
- [50] S. T. Roweis and L. K. Saul, “Nonlinear dimensionality reduction by locally linear embedding,” *Science*, vol. 290, no. 5500, pp. 2323–2326, 2000.
- [51] P. Y. Lu, R. Dangovski, and M. Soljačić, “Discovering conservation laws using optimal transport and manifold learning,” *Nature Communications*, vol. 14, no. 1, p. 4744, 2023.
- [52] H. Hofer and E. Zehnder, *Symplectic invariants and Hamiltonian dynamics*. Birkhäuser, 2012.
- [53] M. Balabane, M. A. Mendez, and S. Najem, “Koopman operator for burgers’s equation,” *Physical Review Fluids*, vol. 6, no. 6, p. 064401, 2021.
- [54] C. Tronci and I. Joseph, “Koopman wavefunctions and clebsch variables in vlasov–maxwell kinetic theory,” *Journal of Plasma Physics*, vol. 87, no. 4, p. 835870402, 2021.
- [55] C. Druţu and M. Kapovich, *Geometric group theory*, vol. 63. American Mathematical Soc., 2018.
- [56] N. B. Kovachki, Z. Li, B. Liu, K. Aizzadenesheli, K. Bhattacharya, A. M. Stuart, and A. Anandkumar, “Neural operator: Learning maps between function spaces with applications to pdes,” *J. Mach. Learn. Res.*, vol. 24, no. 89, pp. 1–97, 2023.
- [57] T. Eisner, B. Farkas, M. Haase, and R. Nagel, *Operator theoretic aspects of ergodic theory*, vol. 272. Springer, 2015.
- [58] K. E. Petersen, *Ergodic theory*, vol. 2. Cambridge university press, 1989.
- [59] A. Berlinet and C. Thomas-Agnan, *Reproducing kernel Hilbert spaces in probability and statistics*. Springer Science & Business Media, 2011.
- [60] D. Wu and G.-R. Duan, “Further geometric and lyapunov characterizations of incrementally stable systems on finsler manifolds,” *IEEE Transactions on Automatic Control*, vol. 67, no. 10, pp. 5614–5621, 2021.
- [61] J. Nocedal and S. J. Wright, *Numerical optimization*. Springer, 1999.
- [62] A. Paszke, S. Gross, F. Massa, A. Lerer, J. Bradbury, G. Chanan, T. Killeen, Z. Lin, N. Gimelshein, L. Antiga, A. Desmaison, A. Kopf, E. Yang, Z. DeVito, M. Raison, A. Tejani, S. Chilamkurthy, B. Steiner, L. Fang, J. Bai, and S. Chintala, “PyTorch: An Imperative Style, High-Performance Deep Learning Library,” in *Advances in Neural Information Processing Systems 32* (H. Wallach, H. Larochelle, A. Beygelzimer, F. d’Alché Buc, E. Fox, and R. Garnett, eds.), pp. 8024–8035, Curran Associates, Inc., 2019.
- [63] M. Towers, J. K. Terry, A. Kwiatkowski, J. U. Balis, G. d. Cola, T. Deleu, M. Goulão, A. Kallinteris, A. KG, M. Krimmel, R. Perez-Vicente, A. Pierré, S. Schulhoff, J. J. Tai, A. T. J. Shen, and O. G. Younis, “Gymnasium,” Mar. 2023.

A Important Definitions

Definition (Group). [55] A group is non-empty set G with a binary operation on G , here denoted as " \cdot ", then the group can be written as (G, \cdot) , three axioms need to be satisfied on group:

- *Associativity.* for all a, b, c in G , one has $(a \cdot b) \cdot c = a \cdot (b \cdot c)$;
- *Identity Element.* There exists an element e in G such that, for every a in G , one has $e \cdot a = a$ and $a \cdot e = a$, such an element is unique in a group;
- *Inverse Element.* For each element a in G , there exists an element b in G such that $a \cdot b = e$, the b is unique commonly denoted as a^{-1} .

B Geometric Interpretation of Koopman Operator

In general, a dynamical system in Equation 1 occurs on a manifold denoted as M . Under the assumption of \mathcal{C}^1 -regularity, the manifold induced by the dynamical system equips with a non-vanishing vector field denoted as $Vect(M)$, and a flow map $F_t : M \rightarrow M$. Here, M has the same topological structure as the $\mathcal{S} \times \mathcal{A}$.

Manifold on Koopman. Koopman operator (see Equation 6) acts observables by composition of a flow map, i.e., the time shifts. Although the space of observables in Hilbert space was defined in this research, other choices exist, such as L^2 space. The defined observables g can be regarded as a continuous function compactly supported on the induced manifold M , where $g \in \mathcal{C}^1(M) \cap \mathcal{H}(\mathcal{S}, \mathcal{A})$. The vector field $P : \mathcal{C}^1(M) \rightarrow \mathcal{C}^0(M)$ acts on the observables coincides with Equation 10. The operator theoretical study of a dynamical system is the study of the operator \mathcal{K}_t instead of the original complex structure of manifold M , and the argument can be found in the research of neural operators such as [56].

Eigenfunctions of Koopman. A \mathcal{C}^1 function $g : M \rightarrow \mathbb{C}$, is said to be a Koopman eigenfrequency ω if every $(s, a) \in M$, for all $t \in \mathbb{R}$, $(\mathcal{K}_t g)(s, a) = \exp(i\omega t)g(s, a)$. Under this property, the Pg can be derived as

$$\mathcal{K}_{\Delta t} g = \exp(i\omega \Delta t)g \quad \Leftrightarrow \quad Pg = i\omega g \quad (25)$$

Here, the Fourier series is chosen as a basis to represent the dynamical system in Hilbert space since the original proof of the Koopman operator [18] is based on the Fourier series. Furthermore, linking with ergodic theory from a spectral perspective will be easier. Without loss of generality, the differential 1-form of Koopman was also interpreted from a trigonometrical sums perspective. According to the Equation 25, the Koopman factors the dynamics onto a rotation action $\mathcal{R}_\omega^{\Delta t}$ on \mathbb{T}^n ⁹ with frequency ω , a category diagram is generated to indicate the fact by combining the representation theory as shown in below

$$\begin{array}{ccc} M & \xrightarrow{F_{\Delta t}} & M \\ \downarrow g & & \downarrow g \\ \mathbb{T}^n & \xrightarrow{\mathcal{K}_{\Delta t} \equiv \mathcal{R}_\omega^{\Delta t}} & \mathbb{T}^n \end{array} \quad \mathcal{R}_\omega^{\Delta t} \mapsto \theta + \omega \Delta t \text{ mod } \mathbb{T}^n \quad g = (g_1, g_2, \dots, g_n)$$

The \mathbb{T}^n is a direct extension from the direct sum of $\bigoplus_{i \in [n]} S^1$, and $g = (g_1, g_2, \dots, g_n)$ is the independent for all $i, j \in [n]$. The commutation of the diagram indicates the equivariant property of the Koopman representation of a dynamical system on \mathbb{T}^n , and it allows the embedding of the low dimensional dynamics into flow with an infinite basis. The closure of the span of P can be denoted as orthogonal trigonometrical sums denoted as O . Then, it can be asserted that

$$H(\mathcal{S}, \mathcal{A}) = O \oplus O^\perp \quad (26)$$

According to the Birkhoff mean ergodic theorem [57, 58], the closure span O will be stable. If not, O^\perp will make the system chaotic due to the slow convergence of ergodic averages. In this scenario, the ergodicity and reducibility of the dynamical system need to be assumed (see Assumption c in Section 2.2).

Lie Theory in Koopman. The Koopman operator has natural connections with the one-parameter group in Lie theory. The exponential map, $exp : \mathfrak{g} \rightarrow G$, is an important feature of the Lie group, which connects the Lie algebra and Lie group together. Based on the definition of the Koopman operator above, it is obvious to see that the periods $\omega \in \mathfrak{g}$. In this situation, defining the vector field P on the Lie group g as $P(g) = g_*(\omega)$. P induces a flow as $\mathcal{R}_P^{\Delta t}$ on the group G , and it is equivalent to say the flow maps the point $e \mapsto \exp(\omega \Delta t)$. By the description of the Koopman operator, the following properties can be derived as

- The vector field P on Lie group G is translation invariant;

⁹ n -dimensional Koopman eigenfunctions can map to n -dimensional torus \mathbb{T}^n .

- for all $t \in \mathbb{R}$ and $\omega \in \mathfrak{g}$, the flow map $\mathcal{R}_\omega^{\Delta t} : G \rightarrow G$ is same as $g \mapsto g \exp(\omega \Delta t)$ (dual representation as Equation 6).

After obtaining the relationship of the Lie group and Lie algebra, the diffeomorphism property can be used to solve the problem on the well-defined group instead of the original manifold.

Lie group and Dynamics. The function g can be regarded as a diffeomorphic map connecting the manifold and the lie group. A commutative diagram of the equivariant system under the Lie theory can be represented as

$$\begin{array}{ccc} M & \xrightarrow{F_{\Delta t}} & M \\ \downarrow g & & \downarrow g \\ G & \xrightarrow{\mathcal{R}_\omega^{\Delta t}} & G \end{array}$$

The diagram indicates the diffeomorphism between the manifold M and group G . When the G is a trigonometric series, the group structure is isomorphic to the torus \mathbb{T}^n . (see the description in Eigenfunctions of Koopman).

C Proofs of Main Theorems

This section provides proof of the Lemmas and theorems in the main text.

C.1 Proof of Lemma 1.

Proof. Under the diffeomorphic property defined in Section B, there should be a diffeomorphic map $g : M \rightarrow \mathcal{H}$. Before proving the theorem, the definition pushforward of diffeomorphism needs to be given.

Let ϕ be a diffeomorphism map $\phi : M \rightarrow N$, for a vector field $X \in Vect(\iota)$ and integral curve $\iota : I \rightarrow M$ and corresponding vector field $(\phi_* X)(\iota(t)) \in Vect(\phi(\iota(t)))$, there exists

$$(\phi_* X)(\iota(t)) = d(\phi(\iota(t)))X(t), \quad (27)$$

where ϕ_* is pushforward operator. According to the above definition of pushforward, the pushforward of $g_*(s_t) \in TG$ can be represented as

$$\begin{aligned} g_*(s_t, a_t) &= d(g(s_t, a_t))X(t) \quad (\text{separability of } X(t) \text{ according to Equation (11)}) \\ &= d(g(s_t)) \underbrace{[f(s_t) + B(s_t)a]}_{\equiv X(t)} \\ &= (g_* f)(s_t) + (g_* B)(s_t)a_t \quad (f\text{-linearity of } g_*) \\ &= \underbrace{Pz_t}_{\text{intrinsic tangent field}} + \underbrace{\tilde{B}(z_t)a_t}_{\text{diffeomorphism of controller}} \end{aligned} \quad (28)$$

Where z_t can be regarded as an uncontrolled dynamical system in spectral space, and Pz_t is the intrinsic tangent vector. On the other hand, the $(g_* B)(s_t)$ is the pushforward of the controller operator (which is the exterior derivative), then $\tilde{B}(z)$ is the lifted operator of $B(s)$ defined on the right-hand side of action a .

C.2 Proof of Theorem 1.

Proof. This theorem can be proven from several different angles, and this study adopts a simple approach. Since the sum of trigonometric series induced a reproducing kernel Hilbert space (RKHS), it is not hard to see the V_g and z are both lying in this induced RKHS [59]. By the reproducing properties¹⁰, there exists the fact that

$$\begin{aligned} V^\pi(s) &= \langle V_g^\pi, g(s) \rangle_{\mathcal{H}} \quad (s \mapsto g(s) \in \mathcal{H}, V^\pi \mapsto \langle V_g^\pi, \cdot \rangle_{\mathcal{H}}) \\ &= V_g^\pi(g(s)) = V_g^\pi(z) \end{aligned}$$

where $V_g^\pi \in \mathcal{H}^*$ and $z \in \mathcal{H}$; \mathcal{H}^* is the dual space of \mathcal{H} . It should be noted that the adopted Fourier series can guarantee the isometric to the original space in L^2 , which also indicates the isometric properties in the Loss function (15).

¹⁰Reproducing properties: for $f \mapsto \langle f, \cdot \rangle_{\mathcal{H}}$, and $x \mapsto k(x, \cdot)$ (k is kernel function), it has the relation $f(x) = \langle f, k(x, \cdot) \rangle_{\mathcal{H}}$

C.3 Proof of Theorem 2.

Proof. In this case, the proof will be decomposed into two cases, one to prove a general case and another to prove the solution of the special quadratic form of the reward function.

Case 1. general form.

By the Bellman optimality, the optimal value function can be represented as a similar form in Equation 18,

$$B^*V(s_t) = \max_{a_t} r(s_t, a_t) + \gamma V(F_{\Delta t}(s_t)). \quad (29)$$

According to the Theorem 1, there exists an equivariant representation in observable space as

$$B^*V_g(z_t) = \max_{a_t} r_g(z_t, a_t) + \gamma V_g(\mathcal{K}_{\Delta t}(z_t)) \quad (30)$$

In this scenario, it assumes that the value function $V \in C^1(M, \mathbb{R})$, then $V_g \in C^1(\mathcal{H}, \mathbb{R})$.

By the definition of the HJB equation [43], the standard form exists:

$$V(x(t + \Delta t), t + \Delta t) = V(x(t), t) + \frac{\partial V(x(t), t)}{\partial t} \Delta t + \frac{\partial V(x(t), t)}{\partial x} \cdot \dot{x}(t) \Delta t + o(\Delta t) \quad (31)$$

where $x(t)$ is the state at time t , since in the value function is time-independent, the $\frac{\partial V(x(t), t)}{\partial t} = 0$. Back to the case, the integral form can be obtained as:

$$\begin{aligned} V_g(\mathcal{K}_{\Delta t}(z_t)) &= V_g(z_t) + \int_0^{\Delta t} \mathcal{L}_{X_g} V_g(z_\tau) d\tau + o(\Delta t) \\ &\approx V_g(z_t) + \nabla_{z_t} V_g^T(z_t) \cdot X_g(\iota(t)) \Delta t + o(\Delta t) \end{aligned} \quad (32)$$

The Lie derivative $\mathcal{L}_{X_g} V_g(z_\tau)$ interprets the change value function $V_g(z_\tau)$ under the vector field of $X_g(t) \in Vect(g(M))$. Instead of searching for a direction in Euclidean space, $\mathcal{L}_{X_g} V_g(z_\tau)$ can be understood as the change of equivariant function along with the vector $X_g(t)$ [60] on equivariant geometry. When the Δt is sufficiently small, the second line of Equation (32) holds. Observing the right-hand side of Equation (30) can be replaced by Equation (32), the following equation can be obtained as

$$\begin{aligned} B^*V_g(z_t) &= \max_{a_t} r_g(z_t, a_t) + \gamma V_g(\mathcal{K}_{\Delta t}(z_t)) \\ &= \max_{a_t} r_g(z_t, a_t) + \gamma (V_g(z_t) + \nabla_{z_t} V_g^T(z_t) \cdot X_g(\iota(t)) \Delta t + o(\Delta t)) \\ &= \max_{a_t} r_g(z_t, a_t) + \gamma V_g(z_t) + \gamma \nabla_{z_t} V_g^T(z_t) [Pz_t + \tilde{B}(z_t)a_t] \Delta t + o(\Delta t) \end{aligned} \quad (33)$$

where the vector field of $X_g(\iota(t))$ is defined as in Equation (12). Typically, the reward function can be decomposed into two separable functions defined by state and action. Here, the r_g can be defined as

$$r_g(z, a) = R_1(a) + R_2(z) \quad (34)$$

where R_1 and R_2 are two independent functions. Plug-in the Equation (34) into the Equation (32), the following form exists:

$$\begin{aligned} &\max_{a_t} r_g(z_t, a_t) + \gamma V_g(z_t) + \nabla_{z_t} V_g^T(z_t) [Pz_t + \tilde{B}(z_t)a_t] \Delta t + o(\Delta t) \\ &= \max_{a_t} R_1(a_t) + R_2(z_t) + \gamma V_g(z_t) + \gamma \nabla_{z_t} V_g^T(z_t) [Pz_t + \tilde{B}(z_t)a_t] \Delta t + o(\Delta t) \\ &= \max_{a_t} \underbrace{R_1(a_t) + \nabla_{z_t} V_g^T(z_t) [Pz_t + \tilde{B}(z_t)a_t] \Delta t}_{\text{dependent on action}} + R_2(z_t) + \gamma V_g(z_t) + o(\Delta t) \end{aligned} \quad (35)$$

When the R_1 is a convex function, the optimization becomes a convex problem, which can be solved analytically. The derivative of R_1 with respect to a is denoted as $H(a) = \nabla_a \langle R_1, a \rangle$ and the action a can be solved as by

$$a = [\nabla \langle R_1, \cdot \rangle]^\dagger (H(a)) \quad (36)$$

This Equation holds because the $\nabla \langle R_1, \cdot \rangle$ is an operator on the left-side of variables a , $[\nabla \langle R_1, \cdot \rangle]^\dagger$ denoted as the inverse map of the operator $\nabla \langle R_1, \cdot \rangle$. The Equation (35) can be got the gradient zero as

$$\begin{aligned} &\max_{a_t} R_1(a_t) + \nabla_{z_t} V_g^T(z_t) [Pz_t + \tilde{B}(z_t)a_t] \Delta t \\ \Rightarrow &H(a_t) + \nabla_{z_t} V_g^T(z_t) \tilde{B}(z_t) \Delta t = 0 \\ \Rightarrow &a_t^* = -[\nabla \langle R_1, \cdot \rangle]^\dagger (\gamma \nabla_{z_t} V_g^T \cdot \tilde{B}(z_t)) \Delta t \end{aligned} \quad (37)$$

Case 2. quadratic form.

To improve the computational efficiency, we also proposed a more specific form for the quadratic form of the value function. For the reward function, the Equation (34) becomes as

$$r_g(z, a) = -a^T R_1 a \Delta t - z^T R_2 z \Delta t \quad (38)$$

where R_1 and R_2 are symmetric semi-positive definite matrices, their dimensions rely on the dimension of observables and actions. In this case, the value function will also become a quadratic form as

$$V(z) = -(z - z^*)^T M(z) (z - z^*) \quad (39)$$

where z^* is the target state in observable space, $M(z)$ is a positive definite matrix. Correspondingly, the Equation (32) in quadratic form becomes

$$\begin{aligned} V_g(\mathcal{K}_t(z_t)) &= V_g(z_t) + \nabla_{z_t} V_g^T(z_t) \cdot X_g(t) \Delta t + o(\Delta t) \\ &= -(z_t - z^*)^T M(z_t) (z_t - z^*) - 2z_t^T M(z_t) \cdot [Pz_t + \tilde{B}(z_t)a_t] \Delta t \\ &\quad - (z_t - z^*)^T \frac{\partial M(z_t)}{\partial z} (z_t - z^*) \cdot [Pz_t + \tilde{B}(z_t)a_t] \Delta t + o(\Delta t) \end{aligned} \quad (40)$$

Meanwhile, the Equation (33) can be

$$\begin{aligned} B^* V_g(z_t) &= \max_{a_t} r_g(z_t, a_t) + \gamma V_g(z_t) + \gamma \nabla_{z_t} V_g^T(z_{t+1}) [Pz_t + \tilde{B}(z_t)a_t] \Delta t + o(\Delta t) \\ &= \max_{a_t} -a_t^T R_1 a_t \Delta t - z_t^T R_2 z_t \Delta t - \gamma (z_t - z^*)^T M(z_t) (z_t - z^*) - 2\gamma z_t^T M(z_t) \cdot [Pz_t + \tilde{B}(z_t)a_t] \Delta t \\ &\quad - \gamma (z_t - z^*)^T \frac{\partial M(z_t)}{\partial z} (z_t - z^*) \cdot [Pz_t + \tilde{B}(z_t)a_t] \Delta t + o(\Delta t) \end{aligned} \quad (41)$$

Due to the convexity of the Equation (41), the gradient zero obtains the optimal action as

$$\begin{aligned} -2R_1 a_t - 2\gamma z_t^T M(z_t) \tilde{B}(z_t) - \gamma (z_t - z^*)^T \frac{\partial M(z_t)}{\partial z} (z_t - z^*) \tilde{B}(z_t) &= 0 \\ \Rightarrow a_t^* &= -\gamma R_1^\dagger [z_t^T M(z_t) + \frac{1}{2} (z_t - z^*)^T \frac{\partial M(z_t)}{\partial z} (z_t - z^*)] \tilde{B}(z_t) \end{aligned} \quad (42)$$

C.4 Proof of Theorem 3

Lemma 1 (Newton-Raphsom Method [61]). Consider a contraction map $E : Y \rightarrow Y$ and the fixed point $y^* = \lim_{n \rightarrow \infty} E^n(y^0)$ for some initial vector $y^0 \in Y \subset \mathbb{R}^n$ and $y^* = E(y^*)$. The step-wise difference is defined as

$$D(y^k) = E(y^k) - y^k \quad (43)$$

where $\forall y^k \in \mathcal{C}^2$ and the contraction operator E indicates the fact that $\lim_{k \rightarrow \infty} D(y^k) \rightarrow 0$, the Newton's step is to update y^{k+1} as

$$y^{k+1} = y^k - [\nabla D(y^k)^T]^{-1} D(y^k) \quad (44)$$

where $D(y^k)$ is differentiable and the $\nabla D(y^k)$ is an invertible square matrix for all k .

Remark 8. Newton-Raphsom method optimizes the target problem by leveraging the second-order information as $\nabla D(y^k)$ as $\nabla D(y^k) = \nabla^2 y^k(t)$ where $y^k(t)$ the time-dependent curve on the manifold of Y . For example, when y_k is approaching the point y^* , there exists:

$$D(y^k) = D(y^*) + \nabla D(y^k)^T (y^* - y_k) = \int_k^\infty \mathcal{L}_{X(t)} D(y^t) dt \quad (45)$$

Where $D(y^*)$ is zero and $X(t)$ is the vector field defined on the curve of $y^k(t)$. Since the $X(t)$ is the tangent vector of geodesic, it can be represented as the Lie transport. So Newton's method of solving the equation locally as

$$D(y^k) + \nabla D(y^k)^T (E(y^k) - y_k) = 0 \quad (46)$$

is just the differential equation of parallel transport [36].

Proposition 1. (Quadratic convergence of Newton-Raphson.) Under the condition of Lemma 1, every step iteration $y^{k+1} = y^k - [\nabla D(y^k)^T]^{-1} D(y^k)$. When $D(y)$ is C_1 -regularity as $\rho_{\min}(\nabla D(y)) > C_1$ ¹¹ and satisfying the following condition as

$$\|\nabla D(y^n) - \nabla D(y^m)\| \leq C_2 \|y^n - y^m\|, \quad \text{for some compact sets}$$

the convergence rate is quadratic as $\|y^{k+1} - y^*\| = \mathcal{O}(\|y^k - y^*\|^2)$.

Proof.

$$\begin{aligned} & \|y^{k+1} - y^*\| \\ &= \|y^k - [\nabla D(y^k)^T]^{-1} D(y^k) - y^*\| \end{aligned} \quad (47)$$

The error gap $D(y^k)$ can be calculated as variational form

$$D(y^k) = \int_0^1 \nabla D(y^* + t(y^k - y^*)) dt (y^k - y^*) \quad (48)$$

Plug to the Equation 48, we get

$$\begin{aligned} & \Rightarrow \|y^k - y^* - [\nabla D(y^k)^T]^{-1} D(y^k)\| \\ &= \|[\nabla D(y^k)^T]^{-1} \left[[\nabla D(y^k)^T] (y^k - y^*) - D(y^k) \right]\| \\ &= \|[\nabla D(y^k)^T]^{-1} \left[[\nabla D(y^k)^T] (y^k - y^*) - \int_0^1 \nabla D(y^* + t(y^k - y^*)) dt (y^k - y^*) \right]\| \\ &\leq \|\nabla D(y^k)^T\|^{-1} \left\| \int_0^1 [D(y^k)^T] - \nabla D(y^* + t(y^k - y^*)) dt \right\| \|y^k - y^*\| \\ &\leq C_2 \|\nabla D(y^k)^T\|^{-1} \|y^k - y^*\|^2 \\ &\leq \frac{C_2}{\gamma} \|y^k - y^*\|^2 \end{aligned} \quad (49)$$

where it is easy to see the quadratic convergence relationship $\|y^{k+1} - y^*\| = \mathcal{O}(\|y^k - y^*\|^2)$.

Proof of Theorem 3. The proof of quadratic convergence of $\|\tilde{V}_g^{k+1} - V_g^*\| = \mathcal{O}(\|\tilde{V}_g^k - V_g^*\|^2)$ can be a direct result from the Proposition 1. It may not be intuitive to plug into this case directly. Let's give some analysis to connect to the Proposition 1.

This analysis provides a one-step rollout case. The multi-step rollout case can be extended following the one-step rollout. It should be noted that the multi-step rollout can be understood as a larger step size to make the convergence of the equivariant of the value function. The core idea behind Newton's step is to use the second-order information to guide the convergence of value function $V_g^k(\theta)$. The second-order information of $V_g^k(\theta)$ is from the Bellman optimality B^* . By observing Equation (23), one-step Temporal Difference is updated by using $r_g(z_t, a_t^*)$ instead of using $r_g(z_t, a_t)$. The a^* derived from Equation (20) and (21) provide a piece of second-order information; see Equation (46). Equivariant geometry compactly supports the equivariant value function, and well-learned equivariant geometry can boost the convergence of the equivariant value function by differential information. Compared to the conventional RL methods, such as SAC, the policy π is updated incrementally as description in Remark 7, and it is impossible to discover a piece of second-order information to guide the policy.

D Experiment Settings

This section provides the experiment settings in the main text, including the model architectures, environment settings, and implementation details.

D.1 Model Architecture

In the implementations, an autoencoding architecture is employed for Koopman embedding, where the encoder and decoder are symmetric and contain only three Fully Connected (FC) layers each. The performance of the proposed KEEC can be easily verified using a simple design and demonstrates its potential to solve more complex control tasks

¹¹ ρ represents the Eigenvalue of matrix.

with more well-designed neural networks. It is recalled that n, m represents the dimension of the environmental state and input control signal, respectively, whereas d is the dimension of latent space (i.e. the finite approximated dimension of our Koopman operators). For the equivariant value function, two types of model architectures were employed: (1) Multi-Layer Perception (MLP) and (2) Quadratic Form $V_g(z) = (z - z^*)^T R(z)(z - z^*)$ where $R(z) = R^{\frac{1}{2}}(z)^T R^{\frac{1}{2}}(z)$ ensures the positive definiteness and z^* is the encoded optimal state s^* . Specifically, the network structure is listed in Tab.2, including the specific sizes used and the different activation functions.

Table 2: KEEC model architecture in our implementation

Components	Layer	Weight Size	Bias Size	Activation Function
Encoder	FC	$n \times \frac{d}{2}$	$\frac{d}{2}$	Tanh
Encoder	FC	$\frac{d}{2} \times d$	d	Tanh
Encoder	FC	$d \times d$	d	Tanh
Decoder	FC	$d \times d$	d	Tanh
Decoder	FC	$d \times \frac{d}{2}$	$\frac{d}{2}$	Tanh
Decoder	FC	$\frac{d}{2} \times n$	n	Tanh
Value Function (MLP)	FC	$d \times d$	d	ReLU
Value Function (MLP)	FC	$d \times \frac{d}{2}$	$\frac{d}{2}$	ReLU
Value Function (MLP)	FC	$\frac{d}{2} \times \frac{d}{2}$	$\frac{d}{2}$	ReLU
Value Function (MLP)	FC	$\frac{d}{2} \times 1$	1	None
Value Function (Quadratic)	FC	$d \times (d \times d)$	$d \times d$	None

As discussed in the main text, no extra parameters were used for training the two lifted P and B instead of solving the least square minimization problem (13) with an analytical solution to obtain \hat{P} and \hat{B} . The solved solutions in each batch were averaged over all the training data. In evaluation, the two approximated lifted operators $\hat{P} \in \mathbb{R}^{d \times d}$ and $\hat{B} \in \mathbb{R}^{d \times m}$ are loaded into the dynamics model and used in the control tasks. In addition, the total number of parameters in each baseline model is provided in Tab.(3).

Table 3: Number of Parameters in each model

Model	Task	Number of Parameters
SAC	Pendulum	3.7k
MPPI	Pendulum	2.2k
CQL	Pendulum	3.6k
KEEC	Pendulum	3.5k (MLP V_g), 33k (Quadratic V_g)
SAC	Lorenz63	4.0k
MPPI	Lorenz63	2.4k
CQL	Lorenz63	4.0k
KEEC	Lorenz63	3.5k (MLP V_g), 33k (Quadratic V_g)

D.2 Implementation Details

At a high level, KEEC and other baselines are implemented in **Pytorch** [62]. Both training and evaluations were conducted on a consumer laptop with a 10-core Apple M1 CPU with 2.14 GHz and no GPU. A comparison of the evaluation time of each model is provided in Tab.4, which is the average of 100 episodes and ± 1 standard deviation.

Table 4: Summary of average episodic implementation time with ± 1 standard deviations of 100 random initials

	Task	Episodic Implementation Time	Time Horizon T
SAC	Pendulum	$0.04 \pm 0.003s$	500
CQL	Pendulum	$0.02 \pm 0.0002s$	500
MPPI	Pendulum	$5.08 \pm 0.72s$	500
KEEC	Pendulum	$1.02 \pm 0.06s$	500
SAC	Lorenz63	$0.39 \pm 0.003s$	5000
CQL	Lorenz63	$0.17 \pm 0.006s$	5000
MPPI	Lorenz63	$100.08 \pm 3.23s$	5000
KEEC	Lorenz63	$8.69 \pm 0.38s$	5000

D.3 Environment Settings

Swing-up Pendulum. The 'Pendulum-v1' environment in the well-known RL benchmark package **Gymnasium** [63] was used to sample the training trajectories for offline models (MPPI, CQL, KEEC), run interactive training for online model (SAC), as well as evaluate the trained model. Additionally, to match the dynamical system of pendulum motion, we change the default setting for the environment state consisting of $(\cos \theta, \sin \theta, \dot{\theta})$ to $(\theta, \dot{\theta})$.

Lorenz-63 Stabilization. The self-implemented Lorenz-63 stabilization task was integrated into the RL setting by the provided API from Gymnasium [63]. The Lorenz-63 system is forwarded with an applied control signal for each step by integrating with a fourth-order Runge-Kutta solver. The state consists of (x, y, z) and control action a consists of (v_x, v_y, v_z) . Tab.(5) lists the environment details.

Table 5: Environment Settings

Task	Optimal state s^*	Reward	Δt	Max number of steps
Pendulum	$(0, 0)$	$-(\theta^2 + 0.1\dot{\theta}^2 + 0.01a^2)$	0.05	999
Lorenz63	$(8.5, 8.5, 27)$	$-(\ s - s^*\ _2 + 0.01\ a\ _2)$	0.01	None